Figures

Published paper

Jumahat, A., Soutis, C., Jones, F.R., Hodzic, A. (2009) *Fracture mechanisms and failure analysis of carbon fibre/toughened epoxy composites subjected to compressive loading*, Composite Structures, 92 (2), pp. 295-305
http://dx.doi.org/10.1016/j.compstruct.2009.08.010

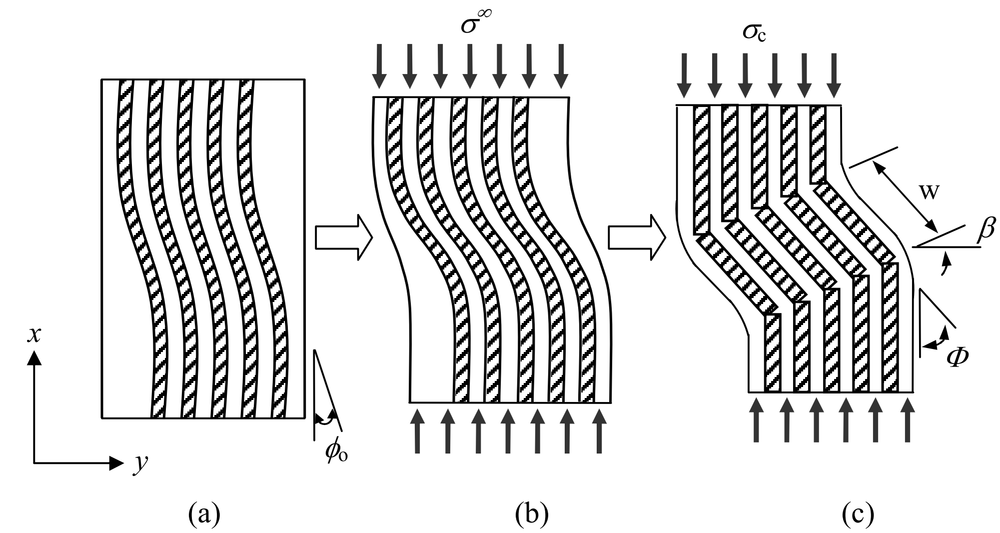

Fig. 1. The schematic diagram showing the formation of kinking failure mode and its geometry; (a) in plane buckling of 0° fibres with an initial fibre misalignment ϕ_o, (b) deformation of 0° fibres via fibre microbuckling mechanism when it is loaded in compression σ^{∞}, and (c) fibres kinking phenomena causing catastrophic fracture of the UD laminate. The kink band geometry: w = kink band width, β = boundary orientation and $\Phi = \phi_o + \gamma$ = inclination angle.

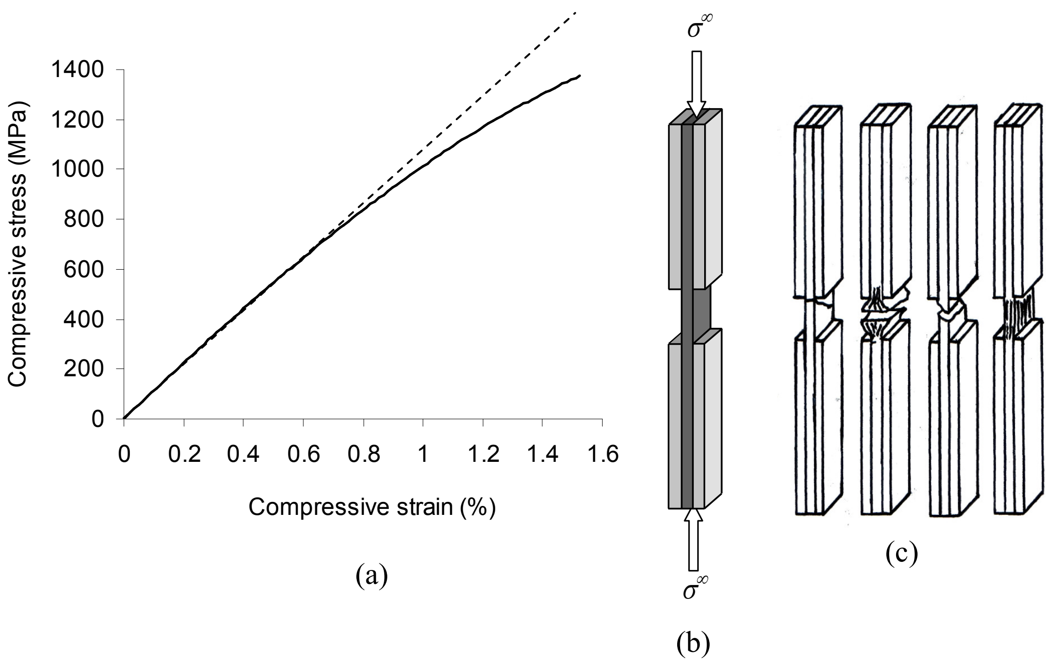

Fig. 2. (a) A typical compressive stress-strain response of a UD HTS40/977-2 laminate [20]; (b) schematic representation of UD specimen loaded in compression; and (c) schematic diagram of various types of failure specimens according to ASTM D3410 and D6641.

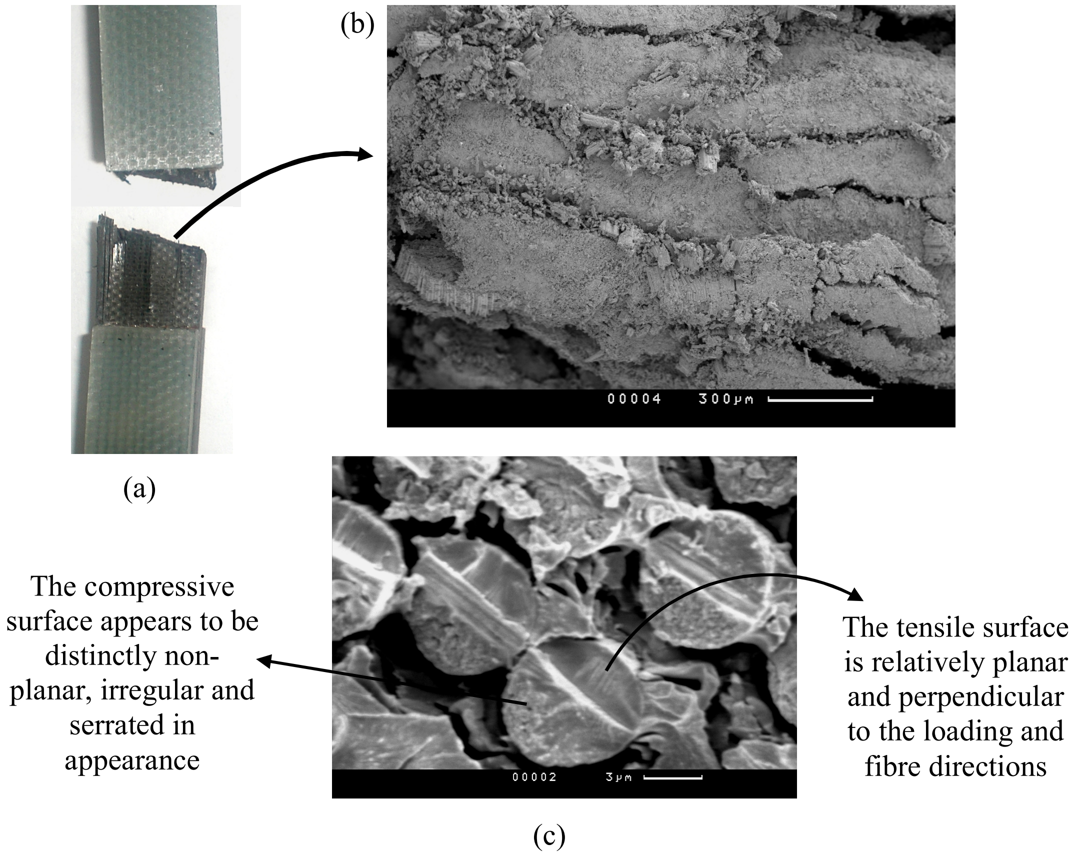

Fig. 3. Characteristics of fractured specimen; (a) the overall view of the actual fractured specimen of UD HTS40/977-2 composite laminate. Fracture surface is at an angle β=10^o to 25^o which is called kink band inclination angle; (b) SEM micrograph of the fractured surface (top view); and (c) SEM micrograph illustrating tensile and compressive surfaces on an individual failed fibre due to microbuckling.

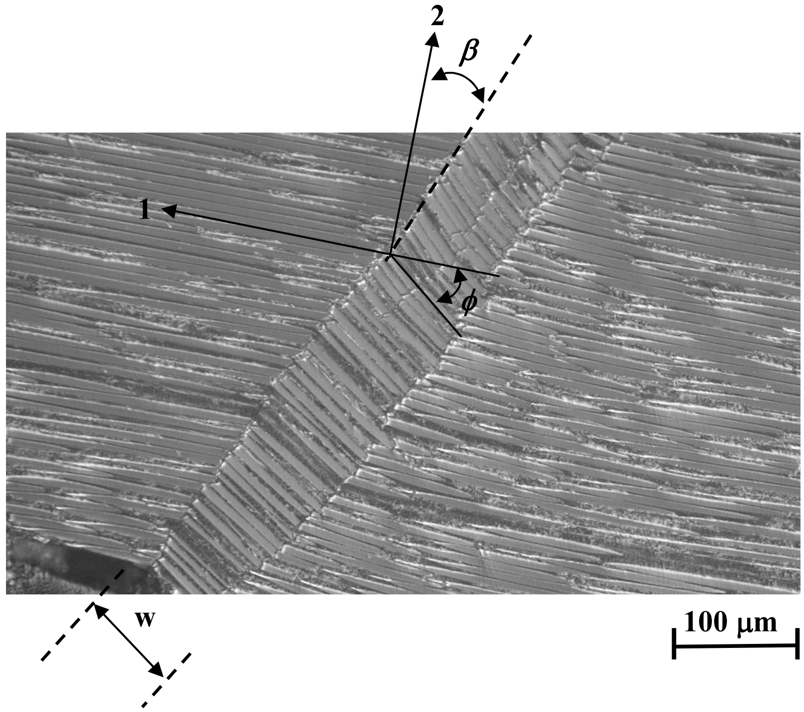

Fig. 4. Optical microscopic across width view (at 200x magnification) of UD HTS40/977-2 CFRP composite laminate. Kink band width, w = 60 μm to 100 μm (or ≈ 8 to 15 fibre diameters) and kink band inclination angle, $\beta = 10^{o}$ to 25^{o}.

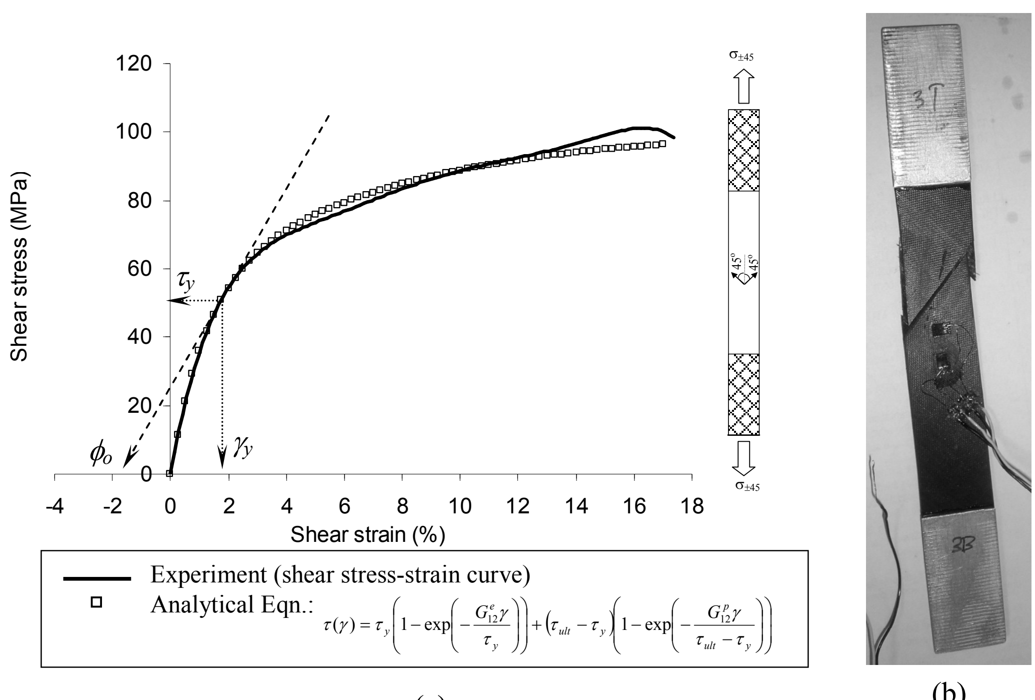

Fig. 5. (a) In-plane shear stress-strain response of a $[\pm 45]_{2s}$ HTS40/977-2 composite laminate and (b) failed specimen.

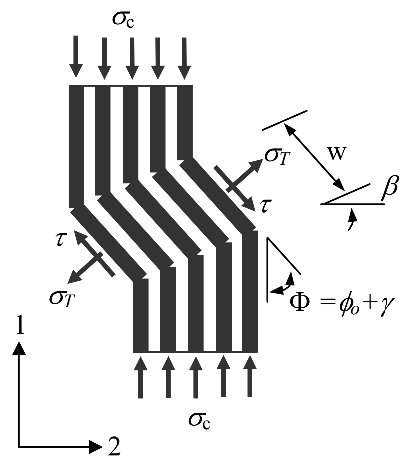

Fig. 6. Budiansky's fibre kinking model with schematic geometry of a kink band width, w oriented at an angle, Φ to the 1-direction (fibre direction) and reaction forces of the material loaded in compression.

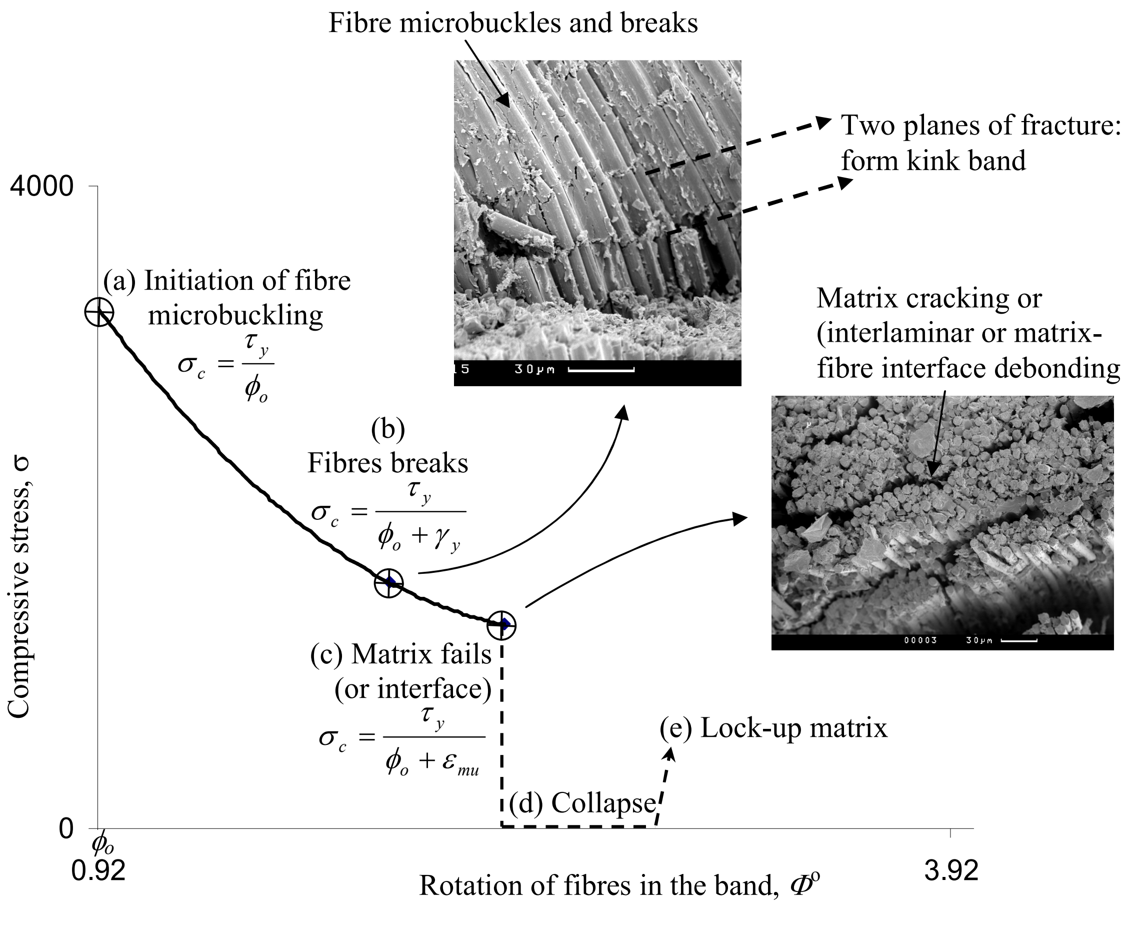

Fig. 7. Theoretical compressive stress-strain response of the UD HTS40/977-2 composite laminate after the initiation of fibre microbuckling.

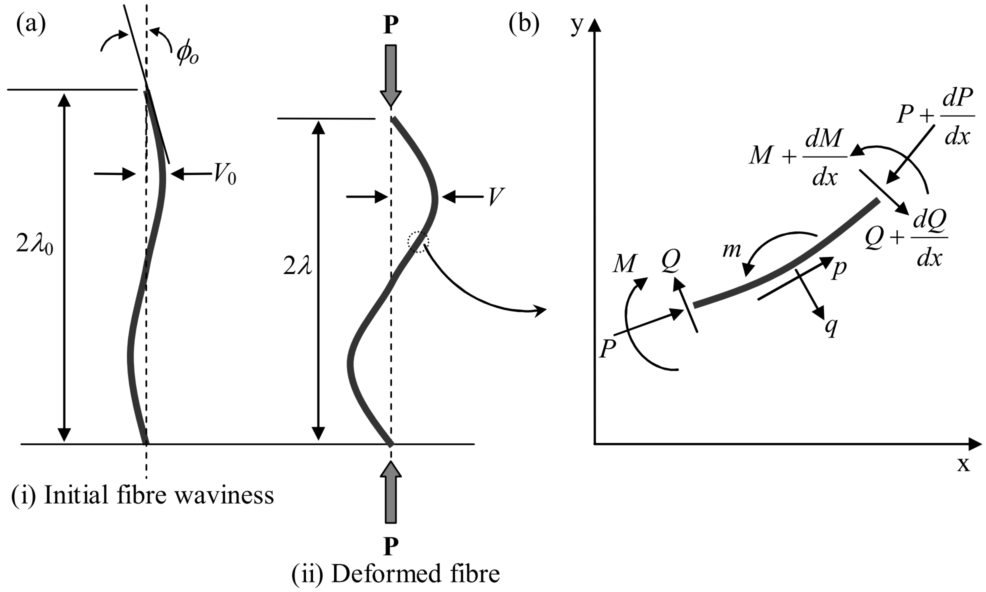

Fig. 8. (a) A schematic of fibre microbuckling mode [24] (b) Free body diagram for a fibre element [4]. P = Axial compressive force, Q = Transverse shear, M = Bending moment, p = Applied distributed axial force, q = Applied distributed transverse force, m = Applied distributed bending moment.

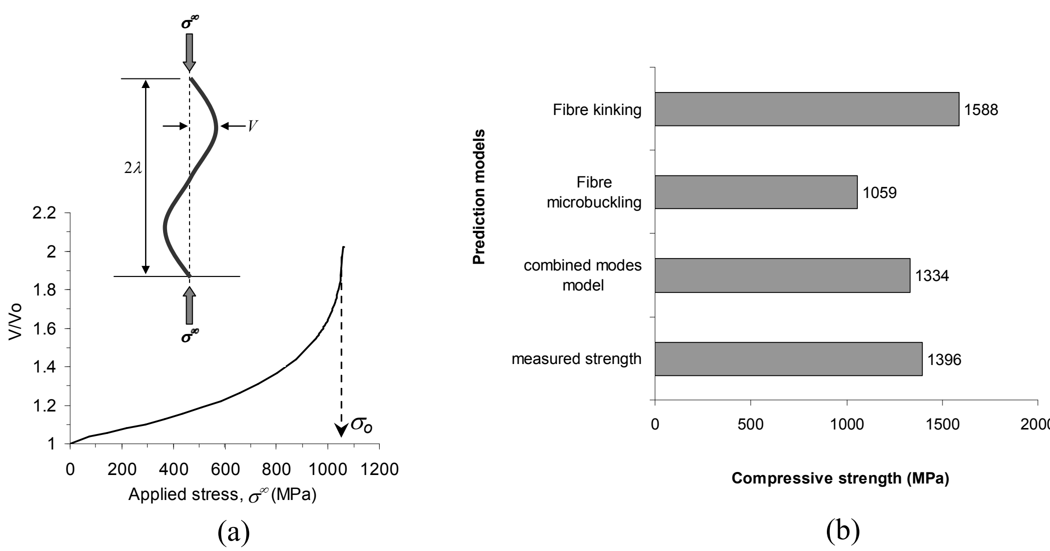

Fig. 9. (a) Fibre amplitude V normalised by initial fibre imperfection V_o versus applied compressive stress, σ^∞. (σ_o =1059 MPa, is the critical stress at which fibre microbuckling is triggered); and (b) compressive strength prediction using combined modes model and comparison between predicted and measured compressive failure strengths of the UD HTS40/977-2 CFRP composite laminate.

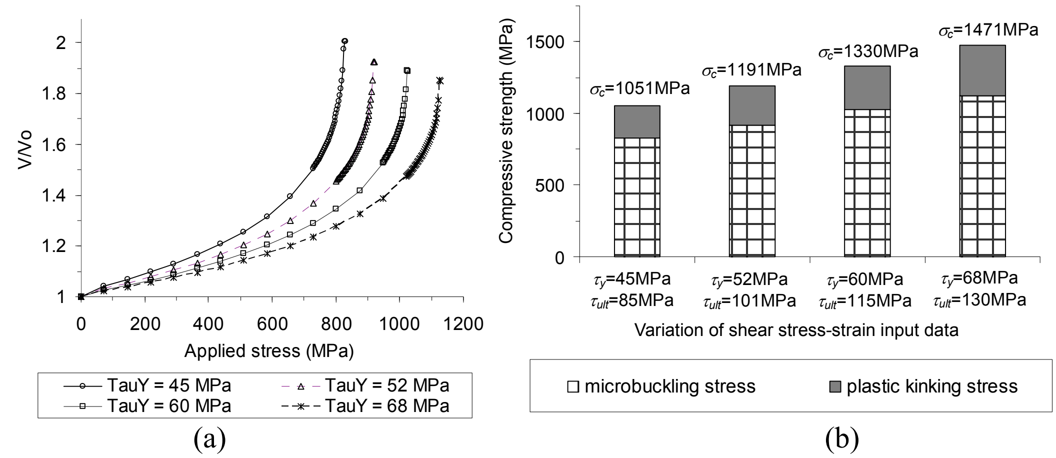

Figure 10: The effects of non-linear shear stress-strain (τ-γ) response on the compressive strength of the UD HTS40/977-2 composite laminate; (a) Variation of 0^o fibre amplitude with applied stress of the UD HTS40/977-2 laminate (b) Compressive strength prediction using combined modes model.

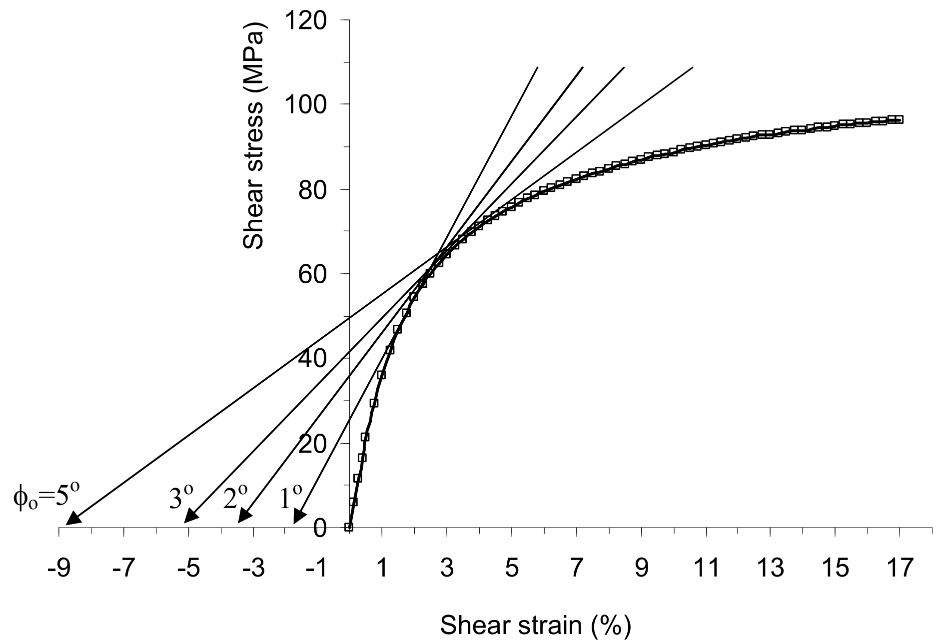

Figure 11: Measurement of shear yield stress and strain using nonlinear shear stress-strain diagram to study the effects of initial fibre misalignment on the compressive strength of the HTS40/977-2 UD composite laminate.

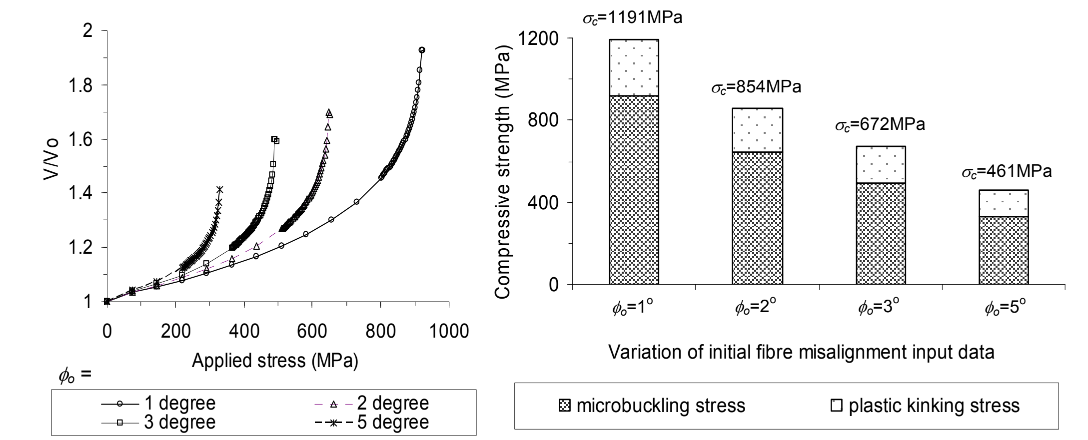

(a) (b)

Figure 12: The effects of initial fibre misalignment on the compressive strength of the UD HTS40/977-2 composite laminates; (a) Variation of 0° fibre amplitude with applied stress on the UD HTS40/977-2 laminate (b) Compressive strength prediction using combined modes model.

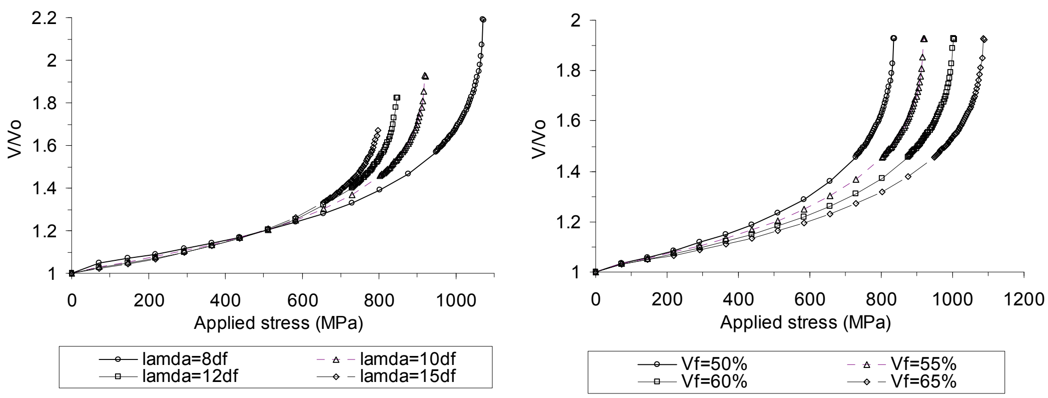

(a) (b)

Figure 13: Variation of 0° fibre amplitude with applied stress on the UD HTS40/977-2 laminate at various (a) initial half-wavelengths of the fibre and (b) fibre volume fractions.

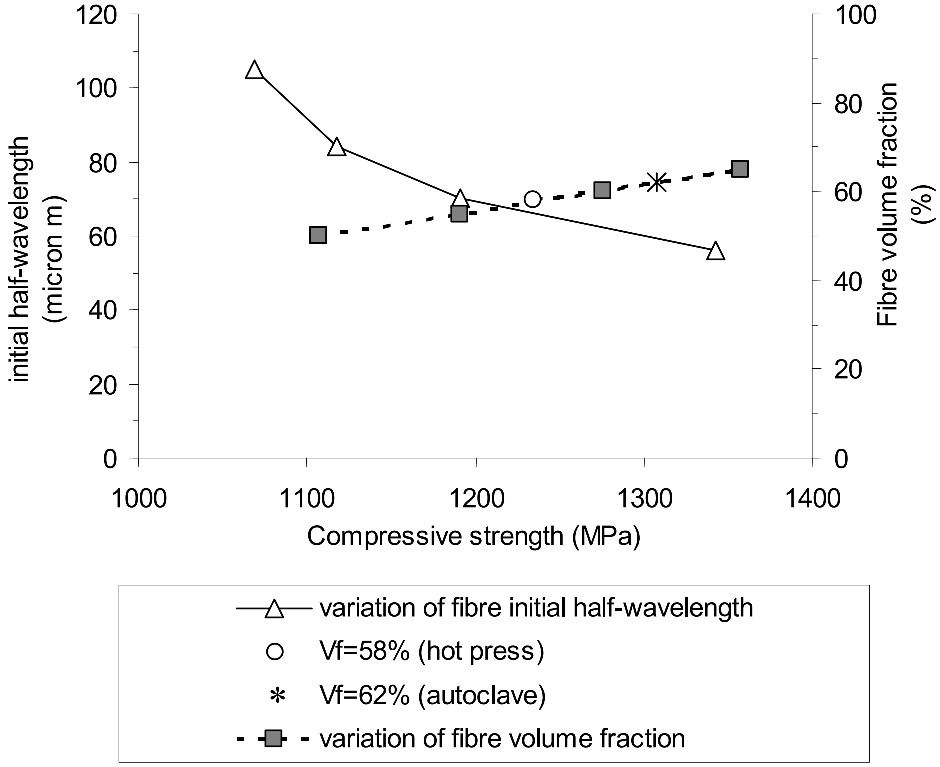

Figure 14: The effects of initial half-wavelength of the fibre and fibre volume fraction on the compressive strength of the UD HTS40/977-2 composite laminates.

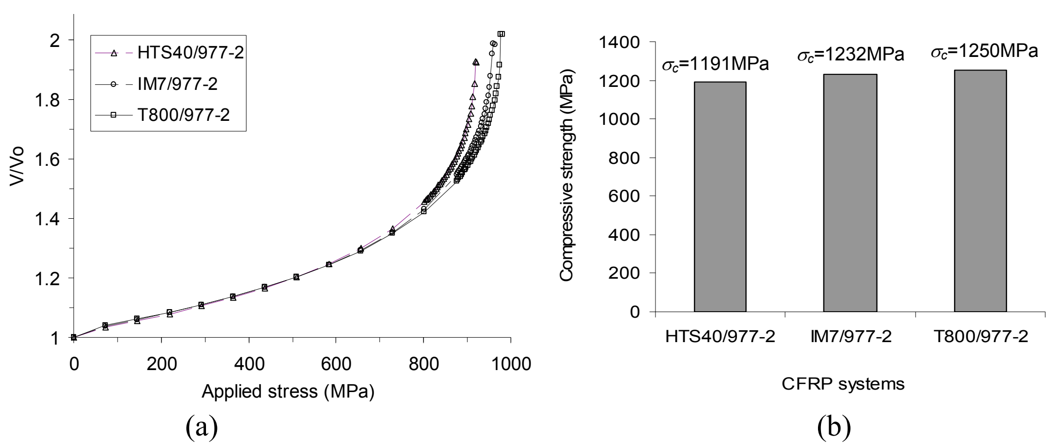

Figure 15: The effects of fibre types and properties on the compressive strength of the UD HTS40/977-2 composite laminate; (a) Variation of 0^o fibre amplitude with applied stress on the UD HTS40/977-2 laminate (b) Compressive strength prediction using combined modes model.